IOP Publishing Physica Scripta
Phys. Scr. 95 (2020) 034002 (11pp) https://doi.org/10.1088/1402-4896/ab5030

Effect of external electric field on multisubband electron mobility in n-V-shaped double quantum well HEMT structure

Ajit K Panda[1], Sangeeta K Palo[1], Narayan Sahoo[2], Trinath Sahu[1] and Tarini Charan Tripathy[3]

[1] Department of Electronics and Communication Engineering, National Institute of Science and Technology, Palur Hills, Berhampur-761 008, Odisha, India
[2] Department of Electronic Science, Berhampur University, Berhampur-760 007, Odisha, India
[3] Department of ECE, Roland Institute of Technology, Berhampur-761 008, Odisha, India

E-mail: narayansahoo.cvrp@gmail.com

Received 28 June 2019, revised 5 October 2019
Accepted for publication 22 October 2019
Published 4 February 2020

Abstract

In this work, we present theoretically the effect of external electric field F_e on low temperature multisubband electron mobility μ in V-shaped double quantum well (V-DQW) HEMT structure. We consider the impact of ionised impurity and alloy disorder scatterings for the calculation of μ. We show that, in the proposed structure, when F_e, is absent, there are two subbands occupied below the Fermi levels. However, as F_e increases, there is an alteration of the potential profile, which changes the energy levels and wave function distributions leading to variation of occupation of subband states, i.e. from double to single. During double subband occupancy, initially, μ enhances with F_e, attains a peak value and then decreases. Whereas, for F_e where the transition from double to single subband occupancy occurs, there is a sudden rise in μ due to the cease of inter-subband interaction. It is interesting to note that different structure parameters, e.g. well widths Ww, central barrier width B_C, doping concentrations N_D, alloy concentrations x_v at the well edges of the V-DQW have a fascinating impact on μ. We show that increasing Ww, and B_C and decreasing N_D, and x_v enhances μ.

Keywords: V-shaped quantum well, external electric field, nonlinear electron mobility, scattering matrix elements

(Some figures may appear in colour only in the online journal)

1. Introduction

Recently, high electron mobility transistor (HEMT) structures with different non-square potential profiles have attracted much attention for the fabrication of electronic and optoelectronic devices due to their specific shapes, like parabolic, cubic, V-shaped, triangular etc [1–25]. These shapes can manipulate the required subband energies and the number of occupation of subband states for specific applications. From these, interests are focused on the development of the devices based on non-square V-shaped quantum well (V-QW) structure due to higher confinement potential [4, 7, 11, 13, 16, 19, 22, 23]. The V-QW structure can be fabricated from $Al_xGa_{1-x}As$ by linearly grading the alloy concentration x inside the well and hence have higher alloy scattering than that of conventional square quantum well (S-QW) structure [13]. In addition to this, in the case of V-QW structure, the higher confinement, as compared to S-QW structure, leads to interesting two-dimensional electron gas properties [26, 27].

A double quantum well (DQW) structure possesses tunnelling coupling in addition to the quantum confinement

effect which can be used to engineer the optical as well as transport properties [1, 3–7, 12, 13, 18, 28, 29]. The coupling of subband states and wave function distributions can be controlled through the proper choice of the central barrier width of the DQW structure. When more than one subband is occupied below the Fermi energy levels, inter-subband interaction comes into the picture [6–8, 27, 29–31].

In general, application of external perturbations like magnetic field F_H, electric field F_e, etc, amends the potential profile $V_{\rm pot}$ of V-QW structure depending upon the magnitude and direction of applied field F_H and F_e. The modified potential profile $V_{\rm pot}$ changes the energy levels and wave function distributions inside the wells, which give rise to interesting optical phenomena [4, 7, 11, 13, 16, 19, 21–23]. For instance, Hu *et al* reported that the effect of F_e on the ground state binding energy for lower well width of V-QW is more significant as compared to that of parabolic quantum well and S-QW structures [8]. Salhi *et al* investigated and presented that the electrical and optical properties of LED operating in the range of 400–500 nm containing V-QW have superior performance as compared to that of the device comprising U-shaped QW [9]. Yesilgul *et al*, have investigated the effect of the strength of the F_H and F_e on the optical absorption coefficients and refractive index of V-QW structure [13]. Radu *et al* presented the effect of laser field on the subband energy levels of the finite V-QW structures under the effect of F_e [19]. Kasapoglu *et al* presented the impact of crossed electric field F_e and Magnetic field F_H on the ground state impurity binding energy of V-QW structure [21]. Boykin *et al* obtained interesting behaviour on the splitting of energy levels in strained V-QW structures in the presence of applied field [22]. There are lots of works available on the application of F_e on optical properties of V-QW structure. However, as per our knowledge, very less work is available regarding the transport properties of V-shaped double quantum well (V-DQW) structures [7, 20].

The electron mobility μ in quantum well structures depends upon the scattering processes related to the system [7, 25, 32–41]. For different temperature regimes, the relevant scattering mechanisms, which play a key role in determining μ, also vary. At low temperatures, the elastic scatterings, such as, ionised impurity scatterings, alloy disorder scattering, interface roughness scattering and acoustic phonon scattering are important in different semiconductor structures, say, GaAs/AlGaAs [32–35]. In case of a system, with an alloy channel (like GaAs/InGaAs structure), the alloy disorder scattering is important [33]. The interface roughness scattering, which arises due to the rough interfaces in heterostructures of dissimilar materials (say, GaAs/$Al_xGa_{1-x}As$), is important in quantum wells of narrow well widths [33, 35–37]. At low temperature the carriers are also scattered by neutral impurities (defect centres) [38]. As temperature increases from 0 K, the effect of acoustic phonon scattering due to deformation potential and piezoelectric interaction increases. The piezoelectric scattering is prominent in compound semiconductors with lack of inversion symmetry [35]. In the case of nitride based quantum well structures (GaN/AlGaN, GaN/InGaN), the strong internal piezoelectric interaction happens to be an essential scattering mechanism to determine the mobility unlike that in arsenide based GaAs/AlGaAs structures [39]. The room temperature mobility is basically governed by the inelastic scattering mechanism, like polar optical phonon scattering [32, 34, 35].

In the present work, we consider $Al_xGa_{1-x}As$ based V-DQW structure in which the side barriers are delta doped with Si. The wells are made of $Al_xGa_{1-x}As$ alloy by varying the alloy concentrations. Unlike the GaAs/$Al_xGa_{1-x}As$ structure, here there is no clear cut interface between the well and the barrier since the whole structure is made of $Al_xGa_{1-x}As$ alloy. We therefore analyse the low temperature mobility governed by ionised impurity scattering and alloy disorder scattering.

We analyse the role of external electric field F_e on multisubband electron mobility in a V-DQW HEMT structure. We show that, in the proposed structure, when F_e, is absent, there are two subbands occupied below the Fermi levels. However, as F_e increases, there is an alteration of the potential profile, which changes the energy levels and wave function distributions leading to variation of occupation of subband states, i.e. from double to single. For multisubband occupancy, μ shows oscillatory behaviour through the imp-scattering. Mobility increases with increasing barrier width, well width and decreasing doping concentration and alloy concentrations at the well edge. In general, for the case of double subband occupancy μ is less than that of single subband occupancy due to additional inter-subband effects. However, with the proper selection of structure parameters and the potential profile it is possible to obtain the reverse trend at the field where single to double subband occupancy occurs. We obtained this by increasing barrier width, well width, doping concentration and also considering asymmetric doping concentrations in both the side barriers. It is our pleasure to reveal that μ of V-DQW rises near the change of the occupation of subbands, i.e. from single to double subbands occupancy, unlike that of square-shaped double quantum well (S-DQW), parabolic-shaped double quantum well (P-DQW), and cubic-shaped double quantum well (C-DQW), where a drop in μ is usually seen. We compared μ of V-DQW with that of P-DQW, and C-DQW and show that μ (C-DQW) $>$ μ (P-DQW) $>$ μ (V-DQW). The obtained results will be helpful for the improvement of the optical as well as transport properties of non-square quantum well based new devices with proper selection of the structure parameters and applied electric field F_e.

2. Theory

2.1. V-DQW HEMT structure

We consider a V-DQW HEMT structure carved from the $Al_xGa_{1-x}As$. The schematic layout of the structure is shown in figure 1(a). Here, the alloy concentration x varies continuously from 0 to x_v ($x_v \leqslant 0.3$) from the centre to the edges of the wells respectively. The barriers are made of $Al_{0.3}Ga_{0.7}As$, with fixed alloy concentration of 0.3. W_F and

W_B are well widths from the front and back sides of the designed structure, respectively. The outside barriers are modulation δ-doped with Si of doping concentrations N_{DF} and N_{DB} of width D_F and D_B at spacer distances S_F and S_B towards the front and back sides, respectively. The wells are separated from each other by the central barrier of width B_C.

The potential profile V_{str} (z) of the V-DQW is:

$$V_{str}(z) = \begin{cases} V_B & z < -(W_B + B_C/2) \\ V_V \left| \dfrac{-z - (B_C + W_B)/2}{W_B/2} \right| & -(W_B + B_C/2) < z < -(B_C/2) \\ V_B & -(B_C/2) < z < (B_C/2) \\ V_V \left| \dfrac{z - (B_C + W_F)/2}{W_F/2} \right| & (B_C/2) < (B_C/2 + W_F) \\ V_B & z > (B_C/2 + W_F) \end{cases}, \quad (1)$$

where V_V and V_B are the potential height at the well boundaries and barrier, respectively. These can be obtained from the conduction band offset presented in table 1. V_V varies from 72 to 228 meV (taking $x = 0.1$–0.3) and $V_B = 228$ meV for $x = 0.3$ [32] [42]. The other parameters such as effective mass, dielectric constant, and lattice constant of $Al_xGa_{1-x}As$ are also presented in table 1.

2.2. Electronic structure

The difference in electron affinity and mismatch in the band alignment leads for the diffusion of electrons into the wells leaving positive ions in the side barriers. So the impurity N_{IMP} (z) and electron distribution n_e (z) towards the growth side of the structure (z-axis) is [27]:

$$N_{IMP}(z) = \begin{cases} N_{DB} & -(S_B + W_B + B_C/2) > z > -(D_B + S_B + W_B + B_C/2) \\ N_{DF} & (S_F + W_F + B_C/2) < z < (D_F + S_F + W_F + B_C/2) \\ 0 & \text{Otherwise} \end{cases}, \quad (2)$$

$$n_e(z) = \sum_n n_n |\psi_n(z)|^2 \qquad -\infty < z < \infty, \quad (3)$$

Ψ_n (z) and E_n (z) of the V-DQW structure satisfies 1D Schrödinger equation towards z-axis [27]:

$$\left[\frac{-\hbar^2}{2m}\frac{d^2}{dz^2} + V_{pot}(z)\right]\psi_n(z) = E_n\psi_n(z), \quad (4)$$

where, m is the effective mass of the electron (table 1), V_{pot} $(z) = V_{str}$ $(z) + V_H$ (z). V_H (z) satisfies Poisson's equation [27]. Application of additional electric field F_e alters the net potential profile $V_{pot}(z)$. Accordingly, another potential $V_F = eF_ez$ is included to V_{pot} (z), in addition to V_{str} (z) and V_H (z). We calculate Ψ_n (z) and E_n (z) numerically by using multistep potential approximation [33, 43]. We show in figure 1(b) the calculated V_{pot} (z), Ψ_n (z) and E_n (z) for the two lowest occupied levels by considering the structure parameters $D_F = D_B = D_D = 20$ Å, $S_F = S_B = S_S = 60$ Å, $W_F = W_B = W_W = 100$ Å, $B_C = 40$ Å, $x_V = 0.3$, $N_{DF} = N_{DB} = N_D = 1 \times 10^{18}$ cm^{-3} and $F_e = 0$ kV cm^{-1}.

We assume that at low temperature all the donors are ionised and diffused into both the adjacent wells. So that the surface electron density $N_{surf} = N_{DF}D_F + N_{DB}D_B$. N_{surf} related to n_n by $N_{surf} = \sum_{n'} n_{n'}$ [27].

2.3. Electron subband mobility

The subband electron mobility μ_n can be expressed in terms of subband life time τ_n, expressed by the electron Fermi energy E_F as $\mu_n(E_F) = (e/m)\,\tau_n(E_{Fn})$. The subband life time τ_n satisfies the coupled linear equation [7, 27]:

$$\sum_{m=0}^{N} G_{nm}\tau_{tm} = 1, \quad (5)$$

which can be derived from the Boltzmann transport equation by employing the Fermi golden rule (see appendix). When a single subband is occupied, equation (5) can be expressed as [37]:

$$\frac{1}{\tau_0} = X_{00}. \quad (6)$$

For double subband occupancy, τ_0 and τ_1 can be expressed as [37]:

$$\frac{1}{\tau_0} = \frac{(X_{00} + Y_{01})(X_{11} + Y_{10}) - Z_{01}Z_{10}}{(X_{11} + Y_{10}) + (E_{F1}/E_{F0})^{1/2}Z_{01}}, \quad (7)$$

$$\frac{1}{\tau_1} = \frac{(X_{00} + Y_{01})(X_{11} + Y_{10}) - Z_{01}Z_{10}}{(X_{00} + Y_{01}) + (E_{F0}/E_{F1})^{1/2}Z_{10}}. \quad (8)$$

Here, X_{nn} is the intra-subband and Y_{nm} and Z_{nm} are inter-subband scattering rate matrix elements (SRMEs). X_{nn}, Y_{nm} and Z_{nm} vary differently for different scattering phenomena (imp/al). The mobility for imp/al scattering can be obtained: $\mu^{imp/al} = \sum_n n_n\mu_n^{imp/al}/\sum_n n_n$. Finally, the whole mobility μ is obtained by the help of Matthiessen's rule i.e. $1/\mu = 1/\mu^{imp} + 1/\mu^{al}$ [27].

2.4. Scattering potential

We can write the intra- and inter-subband SRMEs X_{nn}, Y_{nm}, and Z_{nm} concerning the screened scattering potential $V_{nm}^{SSP}(q_{nm})$:

$$X_{nn} = \frac{m}{\pi\hbar^3}\int_0^{\pi} |V_{nn}^{SSP}(q_{nn})|^2\,(1 - \cos\theta)d\theta, \quad (9)$$

$$Y_{nm} = \frac{m}{\pi\hbar^3}\int_0^{\pi} |V_{nm}^{SSP}(q_{nm})|^2\,d\theta, \quad (10)$$

$$Z_{nm} = \frac{m}{\pi\hbar^3}\int_0^{\pi} |V_{nm}^{SSP}(q_{nm})|^2\cos\theta d\theta. \quad (11)$$

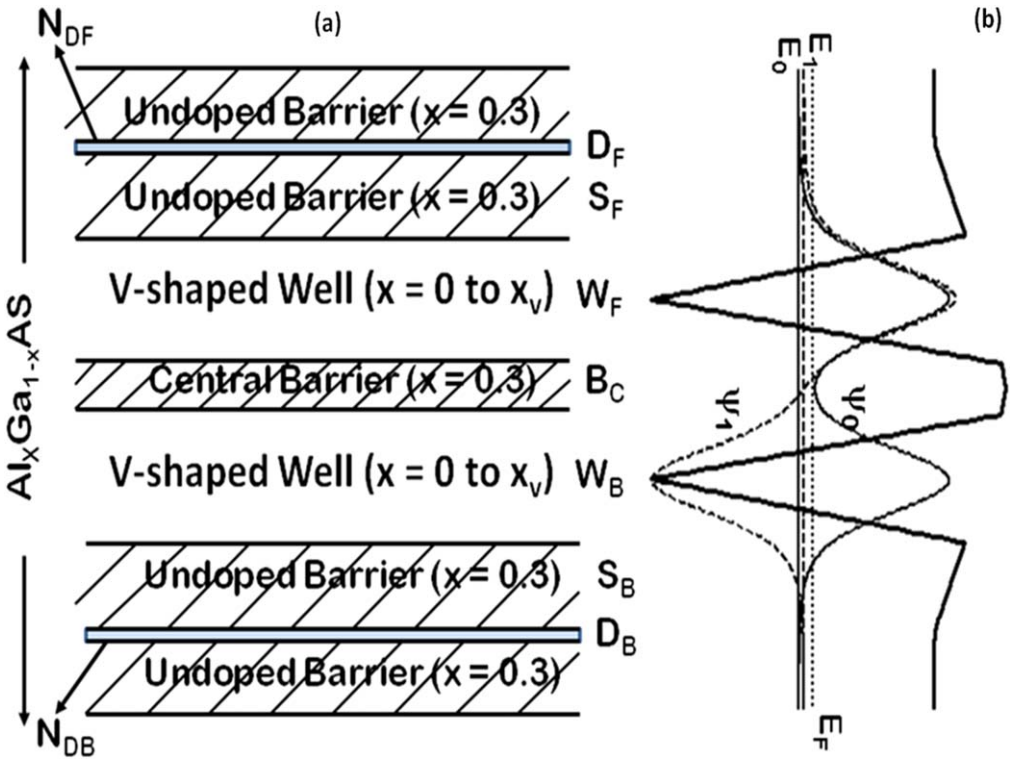

Figure 1. (a) The schematic layout of a symmetric V-shaped double quantum well (V-DQW) HEMT structure made up with $Al_xGa_{1-x}As$. Here B_C: central barrier width, W_F and W_B: well widths, S_F and S_B: spacer widths, D_F and D_B: Doping width, N_{DF} and N_{DB}: Doping concentrations towards the front and back side of the HEMT structure respectively. (b) Represent the shape of the potential and two occupied energy levels E_0 and E_1 and the associated wave function distributions Ψ_0 and Ψ_1 respectively by taking the structure parameters $W_F = W_B = 100$ Å, $S_F = S_B = 60$ Å, $D_F = D_B = 20$ Å, $B_C = 40$ Å, $x_v = 0.3$, $N_{DF} = N_{DB} = N_D = 1 \times 10^{18}\,\mathrm{cm}^{-3}$ and $F_e = 0\,\mathrm{kV\,cm}^{-1}$.

The scattering potentials (imp- and al-) for the V-DQW structure can be expressed as:

$$|V_{nm}^{\mathrm{imp}}(q)|^2 = \frac{4\pi^2 N_{DB} e^4}{\varepsilon_0^2 q^2}\left[\int_{-(D_B+S_B+W_B+B_C/2)}^{-(S_B+W_B+B_C/2)} \mathrm{d}z_i \times \left|\sum_{n'm'} \varepsilon^{-1}_{nm,n'm'}(q) P_{n'm'}(q, z_i)\right|^2\right] + \frac{4\pi^2 N_{DF} e^4}{\varepsilon_0^2 q^2} \times \left[\int_{(S_F+W_F+B_C/2)}^{(D_F+S_F+W_F+B_C/2)} \mathrm{d}z_i \left|\sum_{n'm'} \varepsilon^{-1}_{nm,n'm'}(q) P_{n'm'}(q, z_i)\right|^2\right], \quad (12)$$

where

$$P_{n'm'}(q, z_i) = \int_{-\infty}^{\infty} \mathrm{d}z\ \psi_{n'}(z)\psi_{m'}(z)\mathrm{e}^{-q|z-z_i|}, \quad (13)$$

$$|V_{nm}^{\mathrm{al}}(q)|^2 = \left[\int \mathrm{d}z [\mathrm{a}(z)^3 \delta V(z)^2 x(z)(1 - x(z))/4] \times \left|\sum_{n'm'} \psi_{n'}(z)\psi_{m'}(z)\varepsilon^{-1}_{nm,n'm'}(q)\right|^2\right]. \quad (14)$$

3. Results and discussion

We obtain non-monotonous electron mobility μ through inter-subband interaction in a V-DQW structure. The δ-doped layer widths and spacer widths are $D_F = D_B = D_D = 20$ Å and $S_F = S_B = S_S = 60$ Å. In this work, we consider both the front side well width W_F and back side well width W_B of the proposed structure are same, i.e. $W_F = W_B = W_W$. The maximum heights at the edges of the V-shaped wells i.e. $V_v = 72$, 148 and 228 meV are obtained by taking the alloy concentrations $x_v = 0.1$, 0.2 and 0.3 respectively [42]. For our structure, $\delta V = 1560$ meV, where δV is the alloy disorder scattering potential [44]. We assume F_e negative because it is applied from the back side of the structure. We have used FORTRAN 95 programming language to implement the Schrödinger equation and other equations (equations (6)–(14)) for the calculation of mobility.

Table 1. Material parameters of $Al_xGa_{1-x}As$ used [42].

Sl. No.	Material constant	Value
1.	Effective mass (units of free electron mass m_0)	$m = 0.067 + 0.083x$
2.	Conduction band offset (eV)	$V(x) = 0.693x + 0.222x^2$
3.	Dielectric constant	$\varepsilon = 13.18–3.12x$
4.	Lattice constant (Å)	$a = 5.6533 + 0.0078x$

In figure 2 we present μ^{imp}, μ^{al} and μ ($10^4\,\mathrm{cm}^2\,\mathrm{V}^{-1}\mathrm{s}^{-1}$) by varying F_e ($\mathrm{kV\,cm}^{-1}$) for $W_w = 100$ Å and $B_C = 40$ Å and $N_{DF} = N_{DB} = N_D = 1 \times 10^{18}\mathrm{cm}^{-3}$. The mobility μ is governed by both μ^{imp} and μ^{al}. Initially, for $F_e = 0\,\mathrm{kV\,cm}^{-1}$, two

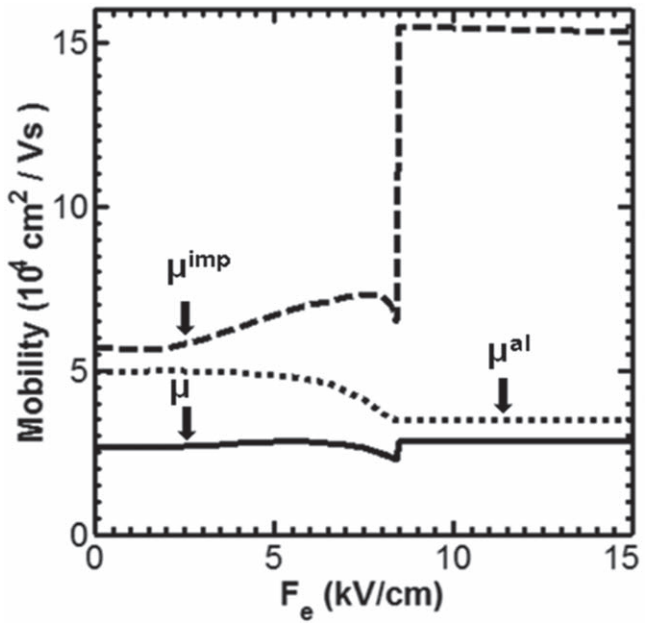

Figure 2. μ^{imp}, μ^{al} and μ as function of F_e of V-DQW structure for $D_D = 20$ Å, $S_S = 60$ Å, $W_W = 100$ Å, $B_C = 40$ Å, $x_v = 0.3$, $N_{DF} = N_{DB} = N_D = 1 \times 10^{18}$ cm^{-3}.

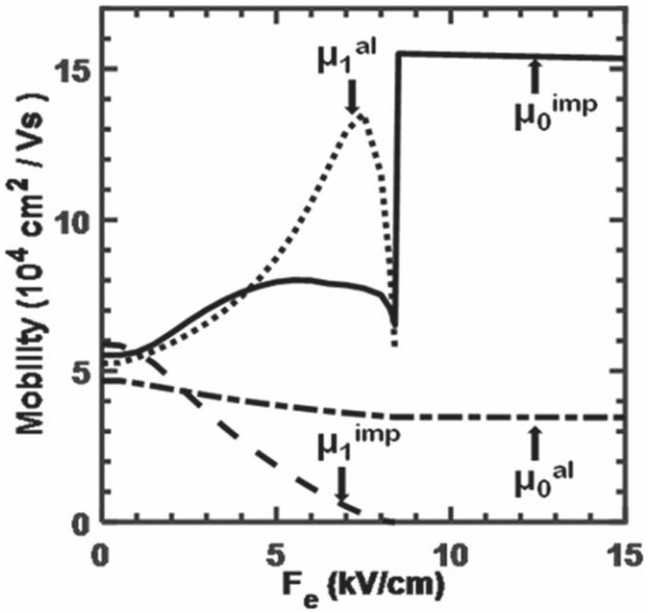

Figure 3. μ_0^{imp}, μ_1^{imp}, μ_0^{al} and μ_1^{al} versus F_e of V-DQW structure with the structure parameters same as that of figure 2.

subbands are occupied which continue up to $F_e = 8.5\,\text{kV cm}^{-1}$. Then only the single subband is below E_F. The absence of inter-subband effect enhances the total mobility. At this transition point, μ^{imp} increases but μ^{al} decreases due to intra-subband effects. For single subband range, μ remains almost constant, but in the double subband range, it fluctuates nonlinearly. Although μ^{imp} causes this fluctuation, μ^{al} governs the overall magnitude of μ.

The behaviour of μ^{imp} and μ^{al} can be explained through their subband mobilities. In figure 3, we present μ_0^{imp}, μ_1^{imp}, μ_0^{al} and μ_1^{al} as a function of F_e. The opposite trends of μ_0^{al} and

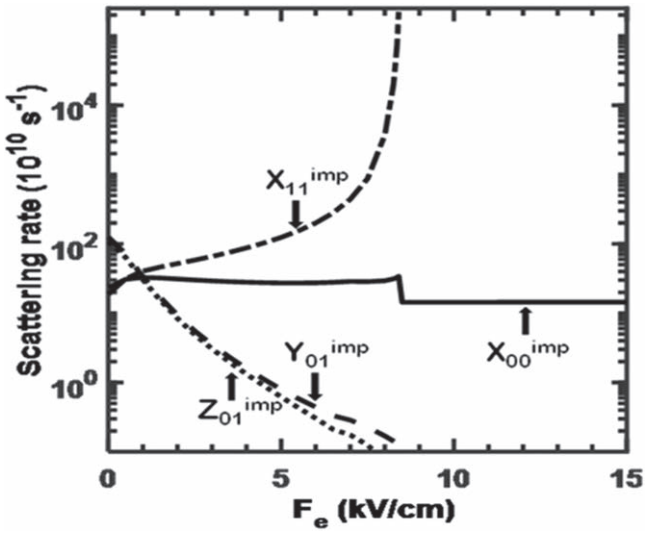

Figure 4. X_{00}^{imp}, X_{11}^{imp}, Y_{01}^{imp}, and Z_{01}^{imp} versus F_e of V-DQW structure with the structure parameters same as that of figure 2.

μ_1^{al}, during the double subband occupancy, make μ^{al} almost flat. From the figure, it is clear that the nonlinear behaviour of μ^{imp} is mainly due to μ_0^{imp}. As the shape of μ mostly depends on μ^{imp}, in figure 4 we present the elements of the scattering rate matrix elements (SRMEs) for imp-scattering, i.e. X_{00}^{imp}, X_{11}^{imp}, Y_{01}^{imp}, and Z_{01}^{imp} as functions of F_e to analyse the nonlinear fluctuation of μ of figure 2. As F_e increases, X_{11}^{imp} increases exponentially wheareas Y_{01}^{imp} and Z_{01}^{imp} decreases exponentially. But X_{00}^{imp} faces little variation during double subband range and maintains constant behaviour during the single subband range. The intra-subband SRMEs X_{00}^{imp} and X_{11}^{imp} play an important role to decide the nonlinear nature in μ when two subbands are occupied in comparison to that of the inter-subband SRMEs Y_{01}^{imp} and Z_{01}^{imp}.

To further illustrate the effect of F_e on mobility, we plot $V_{pot}(z)$, E_0, E_1 and E_F in figure 5(a) and corresponding $\psi_0(z)$ and $\psi_1(z)$ in figure 5(b) for (i) $F_e = 0\,\text{kV cm}^{-1}$, (ii) $8\,\text{kV cm}^{-1}$ and (iii) $15\,\text{kV cm}^{-1}$ taking the structure parameters of figure 2. As F_e increases $V_{pot}(z)$ tilts towards the front side (right side of the figure 5(a)). Accordingly E_0, E_1 and E_F change as shown in the table 2. For $F_e = 0\,\text{kV cm}^{-1}$, structure is symmetric and ψ_0 and ψ_1 extend equally into both the wells in symmetric and antisymmetric manner respectively. Two subbands are occupied (E_F is greater than E_0 and E_1) allowing inter-subband scattering through SRMEs X_{00}, X_{11}, Y_{01}, and Z_{01}. When $F_e \neq 0\,\text{kV cm}^{-1}$, system is potentially asymmetric, ψ_0 lies in the well towards the right side, while ψ_1 lies towards the left well. For $F_e = 8\,\text{kV cm}^{-1}$, even though two levels are occupied, the Fermi level E_F lies just above E_1. The reduced value of $E_{F1} = E_F - E_1$, decreases the subband wave vector q_{nm} (equation (A10)), and hence enhances the scattering potential V_{nm}^{imp} (equation (12)) causing reduction of μ_1^{imp}. Whereas, no such proportionality of q_{nm} occur in V_{nm}^{al} (equation (14)) and the change in μ_1^{al} is mostly due to change in the distribution of the subband wave functions. For $F_e = 15\,\text{kV cm}^{-1}$, single lowest level is occupied, $E_F < E_1$, the mobility is due to intra-subband scattering only.

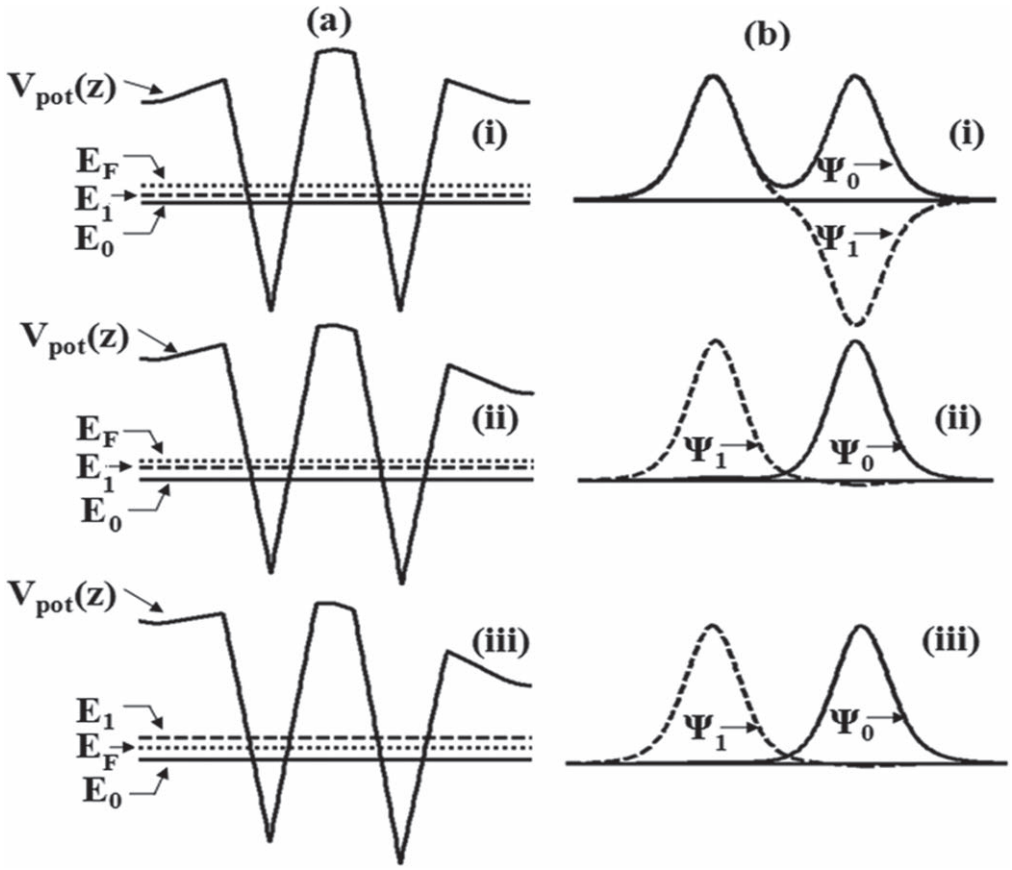

Figure 5. (a). $V_{pot}(z)$, E_0, E_1 and E_F; (b) corresponding $\psi_0(z)$, and $\psi_1(z)$ for (i) $F_e = 0$ kV cm^{-1}, (ii) 8 kV cm^{-1} and (iii) 15 kV cm^{-1} taking the structure parameters same as that of figure 2.

Table 2. Energy levels and mobility due to *imp*- and al-scatterings for different F_e.

	Energy levels (meV)			Mobility (10^4 cm^2 V^{-1} s^{-1})						
F_e (kV cm^{-1})	E_0	E_1	E_F	μ_0^{imp}	μ_1^{imp}	μ^{imp}	μ_0^{al}	μ_1^{al}	μ^{al}	μ
0	134.84	135.47	141.21	5.522	5.885	5.694	4.678	5.253	4.950	2.648
8	112.60	124.07	124.39	7.524	0.603	7.324	3.509	11.519	3.722	2.468
15	92.85	114.32	104.96	15.347	—	15.347	3.463	—	3.463	2.825

μ_0^{imp} enhances considerably while μ_0^{al} almost remains unchanged (figures 3, 4), compared to that of $F_e = 0$ kV cm^{-1} and $F_e = 8$ kV cm^{-1}, leading to net enhancement in μ.

In figure 6, we plot μ versus F_e by considering different middle barrier widths B_C. Here we take $B_C = 40$, and 60 Å for $W_w = 100$ Å and other parameters same as in figure 2. The V-DQW structure is coupled through the central barrier B_C. The coupling strength has an essential effect on μ. As B_C increases, the coupling strength decreases, thereby making the two wells behave independently. As a result for $B_C = 60$ Å, the rise in μ is quite significant. But the range of F_e for which double subband occupancy occurs decreases as compared to $B_C = 40$ Å. The change in μ for $B_C = 40$ and 60 Å is because of the difference in the subband Fermi energy values.

In figure 7, we show μ versus F_e by considering $W_w = 100$, 150 and 200 Å with other parameters remain unchanged as that of figure 2. As W_w decreases, the nonlinearity in μ decreases but the range of two-subband occupancy increases. The decrease in W_w reduces mobility μ due to μ^{imp} and μ^{al}. This is because of the closeness of the diffused electrons (inside the wells) with that of positive ions (left in the side barriers). It leads to higher ionised impurity scattering. We show that for the case of $W_w = 150$ and 200 Å there is an improvement of μ at the shift of one-subband to two-subband occupancy, unlike that of the S-QW structure where a drop in μ is usually seen. This anomalous increase in μ is due to the higher confinement potential in V-QW and dominance of al-scattering as compared to that of imp-scattering. The enhancement of μ increases with an increase in well width, and it is maximum for $W_w = 200$ Å.

In figure 8, we present μ as a function of F_e taking different doping concentrations, $N_D = 1.0$, 1.5 and 2×10^{18} cm^{-3} for $W_W = 100$ Å, $B_C = 40$ Å and $x_v = 0.3$. Under double subband occupancy, the mobility changes

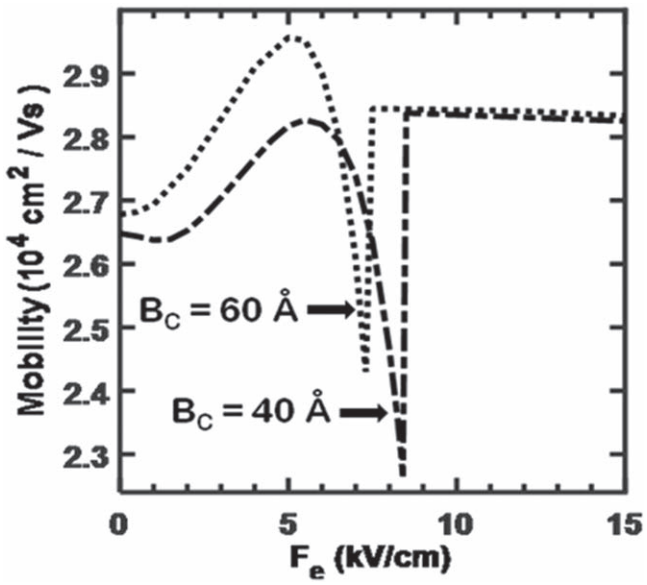

Figure 6. μ versus F_e of coupled V-QW structure for $B_C = 40$ and 60 Å by taking $W_w = 100$ Å. $S_S = 60$ Å, $D_D = 20$ Å, $x_v = 0.3$, $N_D = 1 \times 10^{18}$ cm^{-3}.

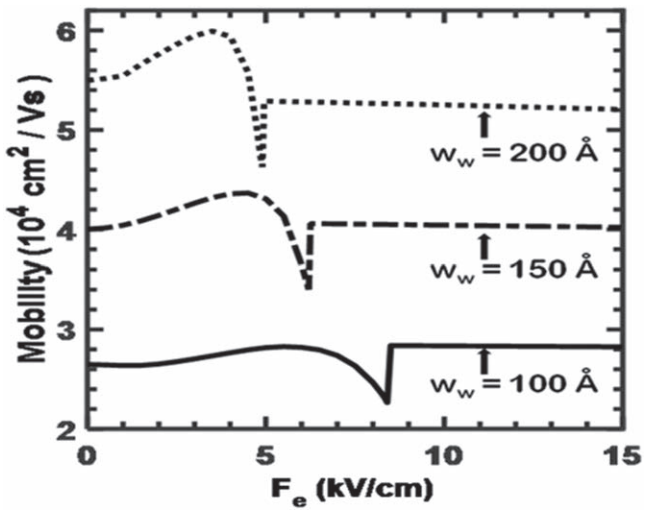

Figure 7. μ versus F_e of V-DQW structure for $W_w = 100$, 150 and 200 Å, with $S_S = 60$ Å, $B_C = 40$ Å, $D_D = 20$ Å, $x_v = 0.3$, $N_D = 1 \times 10^{18}$ cm^{-3}.

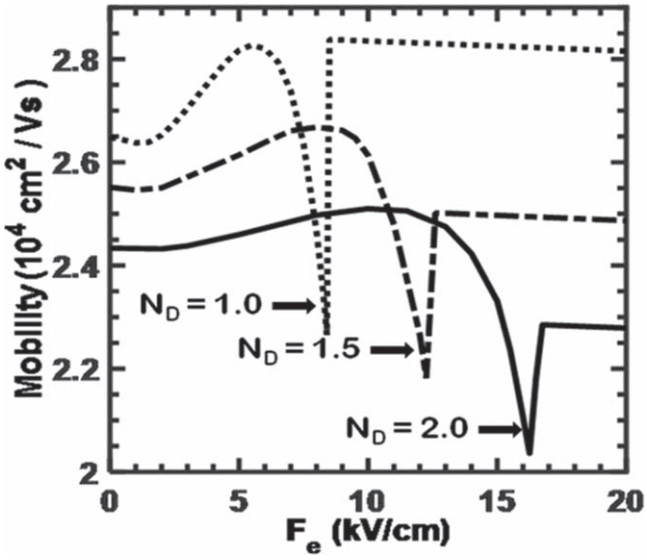

Figure 8. μ versus F_e of V-DQW structure for $N_{DF} = N_{DB} = N_D = 1$, 1.5 and 2 $\times$ 10^{18} cm^{-3} with $W_w = 100$ Å, $S_S = 60$ Å, $B_C = 40$ Å, $D_D = 20$ Å, $x_v = 0.3$.

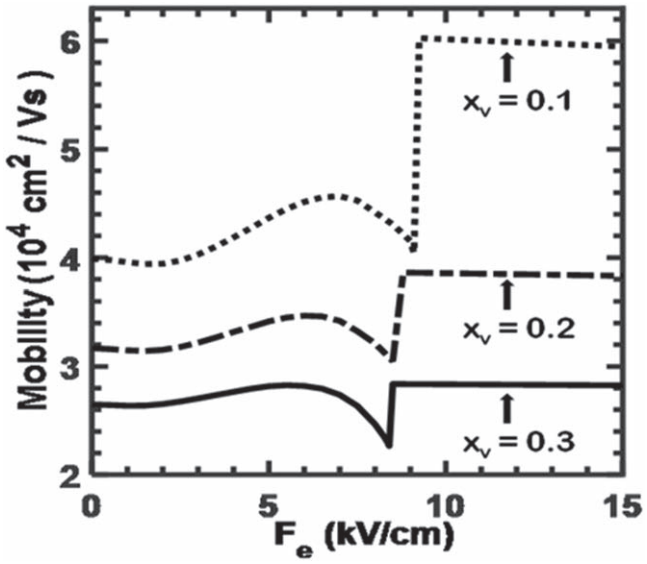

Figure 9. μ versus F_e of V-DQW structure for $x_v = 0.1$, 0.2 and 0.3 with $N_D = 1 \times 10^{18}$ cm^{-3} with $W_w = 100$ Å, with $S_S = 60$ Å, $B_C = 40$ Å, $D_D = 20$ Å.

nonlinearly. This nonlinearity increases as N_D decreases. We show that with the decrease in N_D, μ^{imp} decreases while μ^{al} increases along with a decrease in the range of double subband occupation. We note that as N_D decreases the number of ionised donors decreases. But, simultaneously, the surface electron density also decreases, which attenuates the Fermi wave vector and consequently, Fermi velocity. The afterwards effect being predominating, μ^{imp} decreases with decrease in N_D. Regarding the increase in μ^{al}, we know that as N_D decreases, there is less band bending such that the potential well becomes wider. This makes the amplitudes of the subband wave functions smaller and reduces the al-scattering potential.

In figure 9, we present μ as a function of F_e taking various alloy concentration $x_v = 0.1$, 0.2 and 0.3 with $W_w = 100$ Å for $B_C = 40$ Å, $N_D = 1.0 \times 10^{18}$ cm^{-3}. During double subband occupation, the mobility possesses nonlinearity. For $x_v = 0.1$, mobility faces an abrupt drop at the transition field where single to double subband occupation occur. But this drop gradually reduces as the alloy concentration increases from $x_v = 0.1$–0.2 and then 0.3. We note that as x_v increases the peak in nonlinearity decreases but the transition from single to double subband occupation obtains at a slightly lower value of F_e.

In figure 10, we plot variation of μ with F_e taking different combinations of doping concentrations, (N_{DF}, N_{DB}) = (1, 1), (0.5, 1.5), and (0, 2) $\times$ 10^{18} cm^{-3} with $W_w = 100$ Å, with $S_S = 60$ Å, $B_C = 60$ Å, $D_D = 20$ Å and $x_v = 0.3$. As the difference between the N_{DF} and N_{DB}

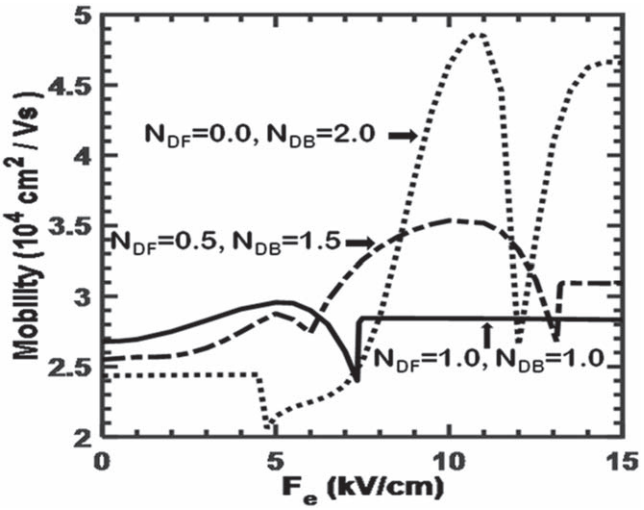

Figure 10. μ as function of F_e for (N_{DF}, N_{DB}) = (1, 1), (0.5, 1.5) and (0, 2) $\times$ 10^{18} cm^{-3} of V-DQW structure for $x_v = 0.3$ with $W_w = 100$ Å, with $S_S = 60$ Å, $B_C = 60$ Å, $D_D = 20$ Å.

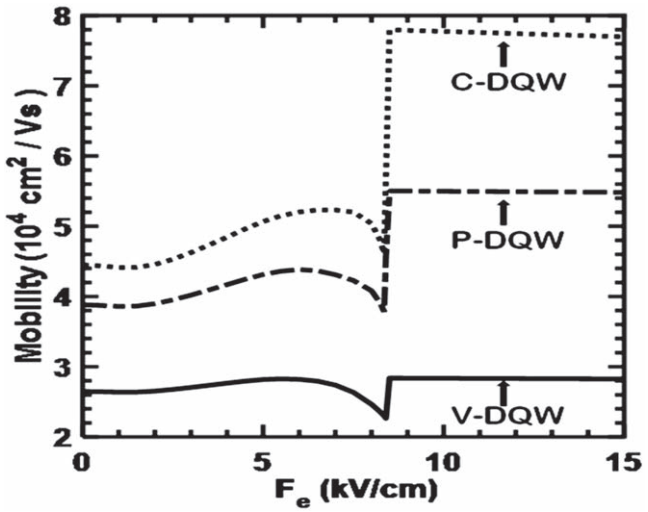

Figure 11. μ as function of F_e in V-DQW, P-DQW and C-DQW structures for $x_v = 0.3$ with $W_w = 100$ Å, $S_S = 60$ Å, $B_C = 60$ Å, $D_D = 20$ Å and $N_D = 1 \times 10^{18}$ cm^{-3}.

increases, μ becomes more nonlinear with large oscillations along negative F_e. We show that for the combination of doping concentrations (N_{DF}, N_{DB}) = (1, 1), and (0.5, 1.5), at first i.e. $F_e = 0$ kV cm^{-1}, there are two subbands occupied. As F_e increases, there is a transition from double to single subband occupancy. It is interesting to show that only in the case of a larger difference between the N_{DF} and N_{DB}, i.e. (N_{DF}, N_{DB}) = (0, 2) $\times$ 10^{18} cm^{-3}, there is single subband occupied followed by double subband. We also calculated and obtained the result of μ for (N_{DF}, N_{DB}) = (0, 2) $\times$ 10^{18} cm^{-3}, by extending F_e up to 20 kV cm^{-1} (Which is not shown in the figure 9) and interestingly at F_e = 16.25 kV cm^{-1} again there is a transition from double to single subband occupancy. There is a fascinating oscillation of μ during the range of second subband occupancy. The oscillation of μ is due to μ^{imp}, but μ^{al} regulates the total magnitude of μ. The applied external field F_e ($\neq 0$ kV cm^{-1}) tilts the whole potential of the quantum well and the structure becomes asymmetric. By varying the difference between N_{DF} and N_{DB}, the potential is changed to realise towards symmetric. For the case (N_{DF}, N_{DB}) = (0, 2) $\times$ 10^{18} cm^{-3} at F_e = F_R = 12 kV cm^{-1} an effectively symmetric potential can be obtained so that the subband states demonstrate resonance. At this point, ψ_0 and ψ_1 extended almost equivalently into both the wells in symmetric and anti-symmetric manner respectively. For $F_e > F_R$ the subband wave functions ψ_0 (ground) and ψ_1 (excited) lie in the left well and right well respectively. For $F_e < F_R$, vice versa occurs. The substantial change in the distribution of $\psi_n(z)$ near $F_e = F_R$, manipulate the scattering potentials significantly. Hence the lowest value of mobility is obtained at $F_e = F_R = 12$ kV cm^{-1}. The larger oscillation in μ is due to the larger nonlinearity of μ_0^{imp} and μ_1^{imp}. The subband mobility μ_0^{imp} almost controls the oscillation of μ^{imp} for $F_e < F_R$ while μ_1^{imp} controls the oscillation for $F_e > F_R$. We show that the resonant point occurs at a lower value of F_e with decreasing the difference between N_{DF} and N_{DB} i.e. for (N_{DF}, N_{DB}) = (0.5, 1.5) $\times$ 10^{18} cm^{-3} F_R = 6 kV cm^{-1}. For the symmetric case with (N_{DF}, N_{DB}) = (1.0, 1.0) $\times$ 10^{18} cm^{-3}, $F_R = 0$ kV cm^{-1}. It is our gratitude to show that for all the three cases, we observe an enhancement of μ near the transition point from single to double subband occupancy.

In figure 11, we show a comparative study for different shaped QW structure potentials like cubic, parabolic and V-shaped. Here, we plot variation of μ with F_e for C-DQW, P-DQW and V-DQW structures for $x_V = 0.3$ with W_w = 100 Å, S_S = 60 Å, B_C = 60 Å, D_D = 20 Å and N_{DF} = N_{DB} = N_D = 1×10^{18} cm^{-3}. We found μ (C-DQW) > μ (P-DQW) > μ (V-DQW). This decreasing trend in mobility is because of the gradually increasing effect of alloy disorder scattering. We note that the sudden drop in μ at the transition field where single to double subband occupation happens for C-DQW and P-DQW can be avoided in the case of V-DQW.

4. Conclusion

Here, we achieve non-monotonous electron mobility μ as a function of external electric field F_e through inter-subband interactions in double V-shaped quantum well HEMT structure. We obtain the asymmetry in the structure by applying an electric field from the back side of the structure. We take ionised impurity (imp-), and alloy disorder (al-) scattering and show the impact of different structural parameters like doping concentrations N_{surf}, central barrier width B_C, well width W_W, and alloy concentration x_v on μ as a function of F_e. Our results show that by increasing B_C and W_W one can improve the non-monotonic nature of μ. The range of F_e, for which double subband occupancy can occur, decreases with increase in N_{surf} but enhances with the decrease of B_C and W_W. The magnitude of μ increases with increasing in B_C, and W_W, whereas decreases with increasing N_{surf} and x_v at the well edges. We show that with a suitable selection of the structure parameters, it is possible to obtain the rise of μ at the

transition of single to double subband occupancy. We also show that the non-monotonic variation of μ during multi-subband occupancy can also be improved more by considering substantial differences in doping concentrations at both the side barriers. We compared the mobility of V-DQW with that of P-DQW and C-DQW and found that V-DQW has higher confinement than that of P-DQW and C-DQW. Our results will be helpful for the improvement of the optical as well as transport properties of non-square quantum well based new devices with proper selection of the structure parameters and applied electric field F_e.

Acknowledgments

SP acknowledges thankfulness for the funding from SERB, Govt. of India through an N-PDF (File No.—PDF/2016/002779).

Appendix

An expression for the electron mobility in a multisubband occupied quantum well system can be derived from the Boltzmann transport equation as [27, 33]:

$$-\frac{e}{m}\hbar\vec{k}\cdot\vec{F}\frac{\partial f_n}{\partial E_{n\vec{k}}} = \sum_{m\cdot\vec{k}'}[S_{m\vec{k}',n\vec{k}}f_m(\vec{k}')[1-f_n(\vec{k})] - S_{n\vec{k},m\vec{k}'}f_n(\vec{k})[1-f_m(\vec{k}')]], \quad \text{(A1)}$$

where $\vec{F}$ is the electric field, $f_n(\vec{k})$ is the electron distribution function of the nth subband. $S_{n\vec{k},m\vec{k}'}$ is the electron transition probability per unit time which is basically derived using the time dependent Schrödinger equation by employing time dependent perturbation formalism [34, 35]. It can be expressed in terms probability of transition from a stationary state $|n\vec{k}\rangle$ to $|m\vec{k}'\rangle$, popularly known as Fermi golden rule:

$$S_{n\vec{k},m\vec{k}'} = \frac{2\pi}{\hbar}\langle|\langle m\vec{k}'|V'|\ n\vec{k}\rangle|^2\rangle\delta_{\vec{k}',\vec{k}+\vec{q}}\delta(E_{m\vec{k}'}-E_{n\vec{k}}), \quad \text{(A2)}$$

where V' the potential of the scatterers. The electronic state $|n\vec{k}\rangle$ can be represented in terms of the wave function and energy eigen values

$$\psi_{n\vec{k}}(\vec{r}) = \frac{e^{i\vec{k}\cdot\vec{\rho}}}{\sqrt{A}}\psi_n(z), \quad \text{(A3)}$$

$$E_{n\vec{k}} = E_n + \varepsilon(k). \quad \text{(A4)}$$

Here $\varepsilon(k) = \hbar^2k^2/2\,m$, $\vec{\rho}$ is the two dimensional position vector along the interface (xy) plane. $\vec{k}$ is the 2D wave vector. A is the area of the sample perpenicular to the growth direction (z-axis). ψ_n is the subband wave functions and E_n is corresponding energy levels of the electron. ψ_n satisfies the Schrödinger equation along z-axis described in equation (4). The Boltzmann equation (equation (A1)) can be expressed as [27, 33]

$$-\frac{e}{m}\hbar\vec{k}.\vec{F}\frac{f_{n\vec{k}}}{\partial\varepsilon} = \sum_m\frac{2\pi}{\hbar}\langle|\langle m\vec{k}'|V'|\ n\vec{k}\rangle|^2\rangle \times\delta(E_n+\varepsilon(\vec{k})-E_m-\varepsilon(\vec{k}'))\delta_{\vec{k}',\vec{k}+\vec{q}}(f_{m\vec{k}'}-f_{n\vec{k}}). \quad \text{(A5)}$$

The outer $\langle.....\rangle$ in the transition matrix relates to the distribution averaging of the scatterers. One can solve equation (A5) exactly by writing the electron distribution function $f_n(\vec{k})$ through the relaxation time approximation, i.e. by introducing energy dependent relaxation time $\tau_n(\varepsilon)$ for each subband [27, 45]:

$$f_n(\vec{k}) = f_n^{(0)}(\vec{k}) + \frac{e}{m}\hbar\vec{k}\cdot\vec{F}\frac{\partial f_n^{(0)}(\vec{k})}{\partial\varepsilon(\vec{k})}\tau_n(\varepsilon) \quad \text{(A6)}$$

f_n^0 is the Fermi–Dirac distribution function and τ_n is the subband transport life time. By using equation (A6) in (A5), the Boltzmann transport equation is obtained in the form of a coupled linear equation in terms of $\tau_n(\varepsilon)$. One can write $\tau_n(\varepsilon) = \tau_n(E_{Fn})$ for $T = 0$ K, where $E_{Fn} = E_F - E_n$. Further, using suitable configurational averaging over the scatterers, the Boltzmann equation can be expressed as (presented in equation (5)):

$$\sum_{m=0}^{N} G_{nm}\tau_m = 1 \quad \text{(A7)}$$

N is the numbers of occupied subbands. G_{nm} is the subband transport scattering matrix:

$$G_{nn} = X_{nn} + \sum_{l\neq n}^{N} Y_{nl} \text{ for } n = m, \quad \text{(A8)}$$

$$G_{nm} = -\frac{k_{Fm}}{k_{Fn}}Z_{nm} \text{ for } n \neq m. \quad \text{(A9)}$$

The intra-subband X_{nn} and inter-subband Y_{nm} and Z_{nm} scattering rate matrix elements can be expressed in terms of the scattering potentials $V_{nm}^{SSP}(q_{nm})$ (as described in equations (9)–(14)). The subband wave vector

$$q_{nm} = [k_{Fn}^2 + k_{Fm}^2 - 2k_{Fn}k_{Fm}\cos\theta]^{1/2}, \quad \text{(A10)}$$

where $k_{Fn} = \left(\frac{2mE_{Fn}}{\hbar^2}\right)^{1/2}\cdot|V_{nm}^{SSP}(q_{nm})|^2 = \langle|\langle m\vec{k}'|V'|\ n\vec{k}\rangle|^2\rangle$ is the configurational averaging of different scattering potential matrix elements including the effect of screening [45].

ORCID iDs

Sangeeta K Palo https://orcid.org/0000-0002-1858-0053
Narayan Sahoo https://orcid.org/0000-0002-8254-6140

References

[1] Bhattacharya P 1996 *Semiconductor Optoelectronic Devices* 2nd edn (New York: Academic)
[2] Ungan F and Bahar M K 2019 The functionality of the external electric and magnetic field on optical specifications of Rosen–Morse quantum well *Phys. Scr.* **94** 085806

[3] Ungan F, Orozco J C M, Restrepo R L, Ramos M E M and Duque C A 2019 Effect of applied electric field on the nonlinear optical properties of modulation-doped $GaAs/Al_xGa_{1-x}As$ double quantum well *Superlattices Microsturct.* **126** 89

[4] Zhang Z H, Yuan J H, Guo K X and Feddi E 2019 Effect of conduction band non-parabolicity on the non-linear optical properties in $GaAs/Ga_{1-x}Al_xAs$ double semi V-shaped quantum wells *Materials* **12** 78

[5] Aydinoglu H S, Sakiroglu S, Sari H, Ungan F and Sokmen I 2018 Nonlinear optical properties of asymmetric double-graded quantum wells *Phil. Mag.* **98** 2151

[6] Ma S, Qu Y and Ban S 2018 Inter-subband optical absorption of electrons in double parabolic quantum wells of $Al_xGa_{1-x}As/Al_yGa_{1-y}As$ *Chin. Phys.* B **27** 027103

[7] Palo S, Sahu T and Panda A K 2018 Effect of non-square structure potential on the multisubband electron mobility in double quantum well structure *Physica* B **545** 62

[8] Hu M, Wang H, Cong Q and Wang S 2018 Comparison of external electric and magnetic fields effect on binding energy of hydrogenic donor impurity in different shaped quantum wells *Eur. Phys. J.* B **91** 19

[9] Abdelmajid A, Mohammad A and Bandar A 2015 Effect of the quantum well shape on the performance of InGaN based light emitting diodes emitting in the 400–500 nm range *J. Display Technol.* **11** 217

[10] Yan T, He J, Yang W, Rajabi K, Chen W, Wu J, Kang X, Zhang G and Hu X 2015 Optical properties of a novel parabolic quantum well structure in InGaN/GaN light emitter *Phys. Status Solidi* a **212** 925

[11] Ozturk E 2015 Nonlinear intersubband transitions in different shaped quantum wells under intense laser field *Superlattices Microsturct.* **82** 303

[12] Choi J K, Vagidov N, Sergeev A, Kalchmair S, Strasser G, Vasko F and Mitin V 2012 Asymmetrically doped GaAs/AlGaAs double-quantum-well structure for voltage tunable infrared detection *Japan. J. Appl. Phys.* **51** 074004

[13] Yesilgul U, Ungan F, Kasapoglu E, Sari H and Sokmen I 2011 The linear and nonlinear intersubband absorption coefficients Effects and refractive index changes in a V-shaped quantum well under the applied electric and magnetic fields *Superlattices Microstruct.* **50** 400

[14] Yang Z, Li R, Wei Q, Yu T, Zhang Y, Chen W and Hu X 2009 Analysis of optical gain property in the InGaN/GaN triangular shaped quantum well under the piezoelectric field *Appl. Phys. Lett.* **94** 061120

[15] Zhu L H, Zheng Q H and Liu B L 2009 Performance improvement of InGaN/GaN light-emitting diodes with triangular-shaped multiple quantum wells *Semicond. Sci. Technol.* **24** 125003

[16] Burileanu L M, Niculescu E C, Eseanu N and Radu A 2009 Polarizabilities of shallow donors in inverse V-shaped quantum wells under laser field *Physia* A **41** 856–60

[17] Gao K H, Yu G, Zhou Y M, Zhou W Z, Lin T, Chu J H, Dai N, Thorpe A J S and Austing D G 2009 Transport properties of AlGaAs/GaAs parabolic quantum wells *J. Appl. Phys.* **105** 013712

[18] Chen B, Guo K, Wang R and Zhang Z 2009 Optical second harmonic generation in asymmetric double triangular quantum wells *Superlattices Microstruct.* **45** 125

[19] Radu A, Niculescu E and Cristea M 2008 Laser dressing effects on the energy spectra in different shaped quantum wells under an applied electric field *J. Optoelectron. Adv. Mater.* **10** 2555

[20] Mamani N C, Duarte C A, Gusev G M, Quivy A A and Lamas T E 2006 Magnetotransport in $Al_xGa_{x-1}As$ quantum wells with different potential shapes *Braz. J. Phys.* **36** 336–9

[21] Kasapoglu E and Sokmen I 2005 Shallow donor impurity binding energy in the V-shaped quantum well under the crossed electric and magnetic field s *Physica* E **27** 198

[22] Boykin T B, Klimeck G, Allmen P V, Lee S and Oyafuso F 2005 Valley spitting in V-shaped quantum wells *J. Appl. Phys.* **97** 113702

[23] Ozturk E, Sari H and Sokmen I 2004 Shallow donor impurity binding energy in the V-shaped quantum well under the crosses electric and magnetic fields *Solid State Commun.* **132** 497

[24] Choi R J, Hahn Y B, Shim H W, Han M S, Shu E K and Lee H J 2003 Efficient blue light-emitting diodes with InGaN/GaN triangular shaped multiple quantum wells *Appl. Phys. Lett.* **82** 2764

[25] Seraide R M and Hai G Q 2002 Low-temperature electron mobility in parabolic quantum wells *Braz. J. Phys.* **32** 344

[26] Harrison P and Valavanis A 2016 *Quantum Wells, Wires and Dots: Theoretical and Computational Physics of Semiconductor Nanostructures* 4th edn (New York: Wiley)

[27] Ando T, Fowler A B and Stern F 1982 Electronic properties of two-dimensional systems *Rev. Mod. Phys.* **54** 437

[28] Silotia P, Giri R and Prasad V 2016 Engineering optical properties of double quantum well systems *Indian J. Pure Appl. Phys.* **54** 641

[29] Ferreira R and Bastard G 1997 Tunneling and relaxation in semiconductor double quantum wells *Rep. Prog. Phys.* **60** 345

[30] Sahoo N, Panda A K and Sahu T 2017 Electron mobility in $Al_xGa_{1-x}As$ based square-parabolic double quantum well HEMT structure effect of asymmetric doping profile *Phys. Status Solidi* b **254** 1700221

[31] Sahoo N and Sahu T 2016 Mobility modulation in inverted delta doped coupled double quantum well structure *Physica* B **498** 49

[32] Walukiewicz W, Ruda H E, Lagowski J and Gatos H C 1984 Electron mobility in modulation-doped heterostructures *Phys. Rev.* B **30** 4571

[33] Bastard G 1988 *Wave Mechanics Applied to Semiconductor Structures* (New York: Halsted Press)

[34] Davies J H 1997 *Physics of Low-Dimensional Semiconductors: An Introduction* (Cambridge: Cambridge University Press)

[35] Lundstrom M 2000 *Fundamentals of Carrier Transport* (Cambridge: Cambridge University Press)

[36] Li J M, Wu J J, Han X X, Lu Y W, Liu X L, Zhu Q S and Wang Z G 2005 A model for scattering due to interface roughness in finite quantum wells *Semicond. Sci. Technol.* **20** 1207

[37] Sahu T and Shore K A 2009 Multi-Interface roughness effects on electron mobility in a $Ga_{0.5}In_{0.5}P/GaAs$ multisubband coupled quantum well structure *Semicond. Sci. Technol.* **24** 095021

[38] Kozhevnikov M, Ashkinadze B M, Cohen E and Ron A 1995 Low-temperature electron mobility studied by electron resonance in ultrapure GaAs crystals *Phys. Rev.* B **52** 17165

[39] Yu T H and Brenann K F 2001 Theoretical study of the two-dimensional electron mobility in strained III-nitride heterostructures *J. Appl. Phys.* **89** 3827

[40] Lima F M S, Fonseca A L A, Nunes O A C and Fanyao Q 2002 Electric field effect on electron mobility in n-AlGaAs/GaAs/AlGaAs single asymmetric quantum wells *J. Appl. Phys.* **92** 5296

[41] Inoue K and Matsuno T 1993 Electron mobilities in modulation-doped $Al_xGa_{1-x}As/GaAs$ and pseudomorphic $Al_xGa_{1-x}As/ In_yGa_{1-y}As$ quantum-well structures *Phys. Rev.* B **47** 3771

[42] Adachi S 1985 GaAs, AlAs, and $Al_xGa_{1-x}As$: material parameters for use in research and device applications *J. Appl. Phys.* **58** R1
[43] Ando Y and Itoh T 1987 Calculation of transmission tunneling current across arbitrary potential barriers *J. Appl. Phys.* **61** 1497
[44] Saxsena A K and Adams A R 1985 Determination of alloy scattering potential in $Ga_{1-x}Al_xAs$ alloys *J. Appl. Phys.* **58** 2640
[45] Sahoo N, Panda A K and Sahu T 2017 Enhancement of multisubband electron mobility in square-parabolic asymmetric double quantum well structure *Superlattices Microstruct.* **105** 11